ARTICLE

$Gd(NO_3)(Se_2O_5)\cdot 3H_2O$: A nitrate-selenite nonlinear optical material with a short ultraviolet cutoff edge

Received 00th January 20xx,
Accepted 00th January 20xx

DOI: 10.1039/x0xx00000x

Chao Wu,[a] Longhua Li,[a] Lin Lin,[a] Zhipeng Huang,[a] Mark G. Humphrey,[b] and Chi Zhang*[a]

The first example of rare-earth metal nitrate-selenite nonlinear optical (NLO) crystal, $Gd(NO_3)(Se_2O_5)\cdot 3H_2O$ (**1**), was synthesized by hydrothermal reaction. This compound crystallizes in the noncentrosymmetric space group $P2_12_12_1$, and its structure features two-dimensional (2D) $[Gd(NO_3)(Se_2O_5)]_\infty$ layers, then extending to a pseudo-3D framework linked by hydrogen bonds. **1** exhibits a phase-matchable SHG efficiency of about 0.2 times that of KH_2PO_4 (KDP) and a large laser damage threshold of 236.26 MW/cm^2. UV-Vis-NIR diffuse reflectance spectroscopy study shows that the UV cutoff edge of **1** is 224 nm, which is the shortest value observed among selenite-based NLO materials. The birefringence of **1** is 0.109@1064 nm based on density functional theory calculations. These optical properties render **1** a potential UV NLO material. Theoretical studies using density functional theory have been implemented to further understand the relationship between its optical properties and band structures.

INTRODUCTION

Coherent ultraviolet (UV) sources have found widespread scientific and technological applications in precision manufacturing, military confrontation, and modern scientific machining field.[1-3] Frequency conversion based on nonlinear optical (NLO) crystal is a fundamental technique to obtain high power UV lasers.[4-9] Over the past decades, the $[BO_3]^{3-}$ anionic group with π-conjugated molecular orbitals[10-12] has been proved to be an optimal structural unit for designing UV or deep-UV NLO crystals because of its wide band gap and large microscopic second-order susceptibility.[13-19] The excellent UV NLO crystals include *β*-BaB_2O_4 (BBO),[20] LiB_3O_5 (LBO),[21] and $Sr_2Be_2B_2O_7$ (SBBO).[22] Apart from the $[BO_3]^{3-}$ group, the $[NO_3]^-$ group also possesses an analogous π-conjugated planar triangular structure.[23] A series of nitrate-based NLO materials[24] were reported recently, such as $RE(OH)_2NO_3$ (RE = La, Y, Gd),[25] $Rb_3SbF_3(NO_3)_3$,[26] $Bi_6O_6F_5(NO_3)$[27] and $Pb_{16}(OH)_{16}(NO_3)$,[28] which are of great interest as a new type of NLO materials.

The combination of two or more types of NLO-active structure building units has also been found to be an effective way for creating novel noncentrosymmetric (NCS) crystalline materials with second-harmonic-generation (SHG) properties.[29,30] For example, a series of NLO materials containing two kinds of stereochemically active lone-pair (SCALP) cations were reported, such as Pb_3SeO_5,[31] $Pb_3Zn_3TeP_2O_{14}$,[32] $Pb_2TiOF(SeO_3)_2Cl$,[33] and $Pb_2GaF_2(SeO_3)_2Cl$.[34] The combination of SCALP cations and π-conjugated systems afforded another class of oxide NLO materials, such as $Bi_3TeO_6OH(NO_3)_2$,[35] $Pb_2(SeO_3)(NO_3)_2$,[36] $PbCdF(SeO_3)(NO_3)$,[37] and $Pb_9Te_2O_{13}(OH)(NO_3)_3$.[38] However, the introduction of SCALP cations into material structures usually leads to the red-shift of UV cutoff edge for the resultant materials,[39] thus limiting their further practical applications in the UV region.

The rare-earth cations RE^{3+} (e.g. Sc^{3+}, Y^{3+}, La^{3+}, Gd, and Lu^{3+}) with closed-shell electronic configurations or half-occupied 4f orbitals, especially in comparison with SCALP cations (Bi^{3+}, Pb^{2+}), are suitable counter cation candidates in the design and synthesis of UV NLO materials, which may effectively inhibit the unfavorable d-d or f-f electronic transitions and broaden the transparent region.[40,41] This certainly impels us to focus our research efforts on the rare-earth metal cations in combination with binary NLO-active structure building units for developing new inorganic NLO materials. Herein this study we describe the synthesis of a gadolinium nitrate-selenite $Gd(NO_3)(Se_2O_5)\cdot 3H_2O$ (**1**) via a facile hydrothermal method. **1** crystallizes in the NCS chiral space group $P2_12_12_1$ and possesses a two-dimensional (2D) $[Gd(NO_3)(Se_2O_5)]_\infty$ layer structure, representing the first example of rare-earth metal nitrate-selenite NLO crystal. The nonlinear optical study shows that **1** exhibits a phase-matchable SHG efficiency of about 0.2 × KH_2PO_4 (KDP), a short UV cutoff edge of 224 nm, a moderate birefringence of 0.109@1064 nm, and a large laser damage threshold (LDT) of 236.26 MW/cm^2. To the best of our knowledge, there is thus far no report on the NLO properties of rare-earth metal nitrate-selenite. First-principle calculations

[a] China-Australia Joint Research Center for Functional Molecular Materials, School of Chemical Science and Engineering, Tongji University, Shanghai 200092, China. E-mail: chizhang@tongji.edu.cn
[b] Research School of Chemistry, Australian National University, Canberra, ACT 2601, Australia

†Electronic Supplementary Information (ESI) available: Additional structures, selected bond distances and angles, hydrogen-bonding interactions, XRD pattern of the residual, IR spectra, TGA, band structure and densities of states. CCDC-1858673 for $Gd(NO_3)(Se_2O_5)\cdot 3H_2O$. For ESI and crystallographic data in CIF or other electronic format see DOI: 10.1039/x0xx00000x.

based on density functional theory were performed to explore the relationship between the optical properties and electronic structure, which indicates that $[SeO_3]^{3-}$ and $[NO_3]^-$ groups are the main contributors to the observed optical response.

Experimental section

Reagents

$Gd(NO_3)_3{\cdot}6H_2O$ (Adamas, 99%) and SeO_2 (Acros, 99.8%) were obtained commercially and used as received.

Synthesis of $Gd(NO_3)(Se_2O_5){\cdot}3H_2O$ (1)

A mixture of $Gd(NO_3)_3{\cdot}6H_2O$ (0.451 g, 1.00 mmol), SeO_2 (0.440 g, 4.00 mmol), and deionized water (4 mL) was sealed in a 20 mL autoclave equipped with a Teflon liner. The autoclave was heated at 80 °C for 72 h, followed by a slow cooling procedure to room temperature. After washing with deionized water, colorless plate-like crystals of **1** were isolated using a microscope (70% based on Gd) (Fig. 1a). The crystals of **1** were stable in air for two months. IR spectrum (KBr pellet, cm^{-1}): 3559 (m), 3417 (br, m), 1660 m, 1448 m, 1344 m, 1054 m, 894 m, 840 m, 781 m, 709 m, 580 m, 507 m.

Structural determination

Single-crystal X-ray diffraction data of **1** were collected at room temperature on a Bruker D8 VENTURE CMOS X-ray diffractometer using graphite-monochromated Mo-Kα radiation (λ = 0.71073 Å). APEX II software was applied to collect and reduce data. Absorption corrections were acquired based on a multiscan-type model. The structure was solved by direct methods and refined on F^2 by full-matrix least-squares methods using SHELXTL-97 software package.[42] All non-hydrogen atoms were refined anisotropically. O(6), O(7), and O(8) atoms in **1** were assigned as water molecules based on bond valence sum (BVS) calculations (Table S1†).[43] The structure was checked with PLATON, and no other higher symmetry elements were found.[44] Table 1 summarizes the crystal data and structural refinement parameters for **1**. The atomic coordinates, equivalent isotropic displacement parameters, BVS calculations, selected bond distances (Å) and angles (deg) are collected in Tables S1–S2†.

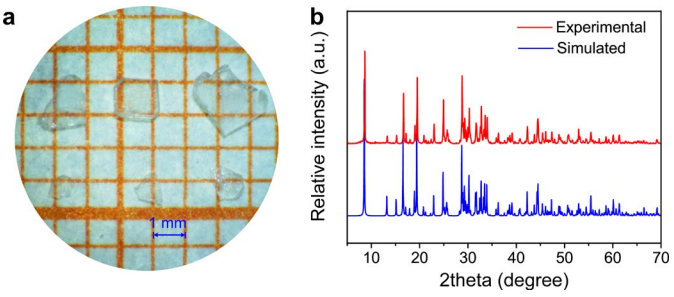

Fig. 1 (a) Crystals photograph of $Gd(NO_3)(Se_2O_5){\cdot}3H_2O$. (b) Powder X-ray diffraction patterns of $Gd(NO_3)(Se_2O_5){\cdot}3H_2O$.

Table 1 Crystallographic data and structure refinement parameters for $Gd(NO_3)(Se_2O_5){\cdot}3H_2O$[a]

Empirical formula	$Gd(NO_3)(Se_2O_5){\cdot}3H_2O$
Formula weight	511.23
Temperature (K)	293(2)
Crystal system	Orthorhombic
Space group	$P2_12_12_1$
a (Å)	6.2509(8)
b (Å)	7.0944(9)
c (Å)	20.747(3)
α (°)	90
β (°)	90
γ (°)	90
Volume (Å^3)	920.1(2)
Z	4
Density (calculated) ($g{\cdot}cm^{-3}$)	3.691
Absorption coefficient (mm^{-1})	15.173
F(000)	932
Theta range for data collection (°)	3.03-27.06
Limiting indices	-8 ≤ h ≤ 7, -9 ≤ k ≤ 9, -26 ≤ l ≤ 26
R_{int}	0.0475
Reflections collected/unique	5408/1992
Goodness-of-fit on F^2	1.110
Final R indices [$F_o^2 > 2\sigma(F_o^2)$][a]	0.0403/0.0815
R indices (all data)[a]	0.0484/0.0842
Largest diff. peak and hole (e Å^{-3})	2.241 and -2.217

[a] $R_1 = \sum||F_o| - |F_c||/\sum|F_o|$; $wR_2 = [\sum w(Fo^2 - Fc^2)^2]/\sum w(Fo^2)^2]^{1/2}$

Powder X-ray diffraction

Powder XRD pattern of **1** was collected on a Bruker D8 X-ray diffractometer with Cu-Kα radiation (λ = 1.5418 Å) in the angular range 2ϑ = 5–70° with a scan step-width of 0.02°. The experimental XRD pattern is shown in Fig. 1b, which indicates that the experimental powder XRD pattern of **1** is in good agreement with the simulated one obtained from the CIF data.

Infrared (IR) spectroscopy

The IR spectrum was recorded on a Nicolet iS10 instrument in the range 400–4000 cm^{-1}. The sample was mixed thoroughly with dried KBr and was then pressed into discs for IR measurements.

UV-Vis-NIR diffuse reflectance spectrum

The UV-Vis-NIR diffuse reflectance spectrum was measured in the range 200–2500 nm at room temperature using a Varian Cary 5000 spectrophotometer. $BaSO_4$ was used as standard. The reflectance spectrum was converted to absorbance according to Kubelka-Munk function: $F(R) = (1-R)^2/2R = \alpha/S$, where R is the reflectance, α is the absorption coefficient, and S is the scattering coefficient.[45]

Thermal analysis

Thermogravimetric analysis (TGA) and differential scanning calorimetry (DSC) of the ground polycrystalline **1** were performed on a Netzsch STA 409PC thermal analyzer instrument. The sample and the reference Al_2O_3 were placed

in platinum crucibles and heated at a rate of 15 °C/min from 30 °C to 900 °C under a flow of nitrogen gas.

Second-Order NLO measurements

The powder SHG response of polycrystalline **1** was evaluated using a modified Kurtz and Perry method.[46] A Q-switched Nd:YAG laser with 1064 nm radiation was employed for visible SHG. The sample **1** was ground and sieved into several particle size ranges (<26, 26−50, 50−74, 74−105, 105−150, 150−200, and 200−280 μm), which were pressed into disks with diameters of 6 mm that were placed between glass microscope slides and secured with tape in a 1 mm thick aluminum holder. Crystalline KDP was also ground and sieved into the same particle size ranges and used as the reference.

Laser damage threshold

The LDTs of **1** and $AgGaS_2$ (as a reference) were measured by the single-pulse method[47] with laser radiation of λ = 1064 nm generated by a Q-switched Nd:YAG solid-state laser. The polycrystalline samples of **1** and $AgGaS_2$ were both ground and sieved into the particle size range of 105−150 μm, and measured based on the same standard. When running the test of LDTs, the power of the incident radiation was increased gradually and slowly until damage spots on sample surface were observed under a magnifier. The LDTs were derived from the equation of $I_{(threshold)} = E/(\pi r^2 \tau_p)$, in which E is the laser energy of a single pulse, r is the spot radius, and τ_p is the pulse width.

Calculation details

All electronic structure calculations were performed using the VASP code[48] within the framework of density functional theory (DFT). The generalized gradient approximation (GGA) function of Perdew-Burke-Ernzerhof (PBE)[49] was employed. A plane wave basis set with a frozen-core projector-augmented wave (PAW)[50,51] potential and a plane-wave cut-off energy of 400 eV was used. A grid of 6 × 6 × 4 Monkhorst-Pack k-points was used for the self-consistent-field convergence of the total electronic energy. The Fermi level was set at zero as the energy reference.

Results and discussion

Crystal Structure of 1.

The first gadolinium nitrate-selenite **1** was successfully obtained by hydrothermal reaction. It crystallizes in an orthorhombic space group $P2_12_12_1$, which is NCS and chiral. The asymmetric unit of **1** includes one Gd, one N, two Se, eleven O, and six H atoms, totaling 21 unique atoms in general sites (Fig. S1†). Gd(1) is eight-coordinated in a square antiprism (Fig. 2a). The bond distances of Gd−O are falling in the range of 2.342(8)−2.491(8) Å. N(1) is coordinated with three oxygen atoms in a $[NO_3]^-$ π-conjugated planar triangle with the N−O distances and O−N−O bond angles ranging from 1.207(13) to 1.278(13) Å and 117.2(10) to 121.7(10)°, respectively. Each Se (Se1 and Se2) atom is connected with three oxygen atoms in a ψ-SeO_3 trigonal pyramid. The Se−O bond lengths are ranging from 1.650(8) to 1.821(8) Å and the O−Se−O bond angles are 93.9(4)−104.2(4)°. BVS calculation results of Gd, Se, N, O are summaried in Table S1†, indicating that the valence states of Gd, Se, N, and O atoms are +3, +4, +5, and −2, respectively.

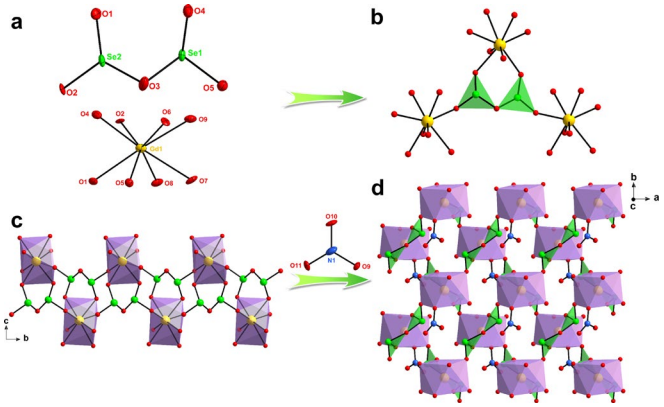

Fig. 2 (a) Crystal structural features of Se_2O_5 and GdO_8 units. (b) Se_2O_5 unit is surrounded by three GdO_8 polyhedra. (c) The 2D $[GdSe_2O_5]_\infty$ layer along the a-axis. (d) The 2D $[Gd(NO_3)(Se_2O_5)]_\infty$ layered structure of $Gd(NO_3)(Se_2O_5)\cdot 3H_2O$ along the c-axis.

The Se_2O_5 unit is comprised of two $[SeO_3]^{2-}$ triangle pyramids connected by sharing one O(3) atom (Fig. 2a). Each Se_2O_5 unit is connected with three GdO_8 polyhedra (Fig. 2b), forming a 2D $[GdSe_2O_5]_\infty$ layer along the a-axis (Fig. 2c). The $[NO_3]^-$ planar triangle is in a monodentate mode, bridging with one Gd atom (Fig. S2†). Specifically, the $[NO_3]^-$ triangles dangle on two sides of the $[GdSe_2O_5]_\infty$ layers via O(9) atoms, forming a 2D $[Gd(NO_3)(Se_2O_5)]_\infty$ layers (Fig. 2d). There are weak hydrogen bonds not only in the $[Gd(NO_3)(Se_2O_5)]_\infty$ layers but also between adjacent chains (Table S3†). The weak hydrogen bonds strengthen the 2D $[Gd(NO_3)(Se_2O_5)]_\infty$ layers to a pseudo-3D framework running down the a-axis (Fig. 3).

Thermal stabilities

The thermalgravimetric (TG) curve of **1** is shown in Fig. S3†, which exhibits two main steps of weight losses. An initial weight loss of 10.60% is observed between 110 and 190 °C,

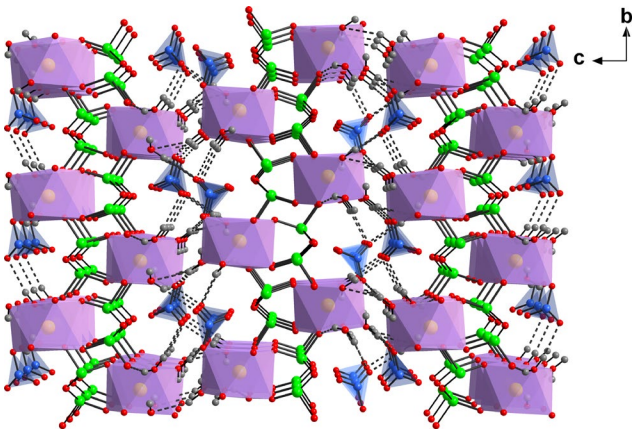

Fig. 3 Pseudo-3D network of $Gd(NO_3)(Se_2O_5)\cdot 3H_2O$ connected by hydrogen bonds.

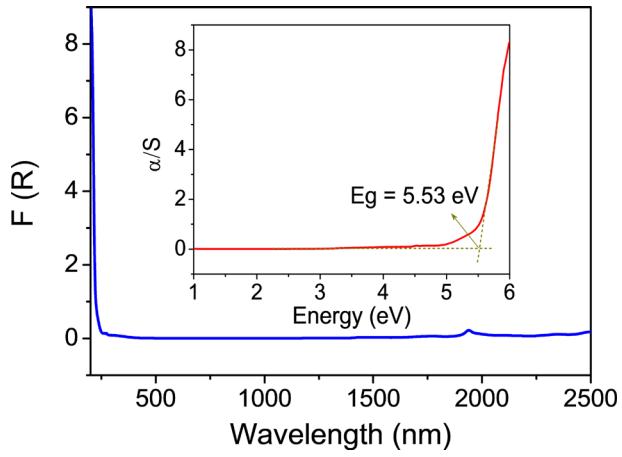

Fig. 4 UV-Vis-NIR diffuse absorption spectra of $Gd(NO_3)(Se_2O_5)\cdot 3H_2O$. The inserts show the corresponding band gap.

which corresponds to the removal of three H_2O molecules (calculated value: 10.57%). The second weight loss of 55.32% occuring between 200 and 850 °C is attributable to the elimination of one NO, one O_2 and two SeO_2 groups (calculated value: 55.54%), which is consistent with the DSC curve of **1**. After these two steps of weight losses, **1** was heated at 900 °C for 2 h and on the basis of the powder XRD studies, the residues were determined to be mainly Gd_2O_3 phase (Fig. S4†).

IR measurements

The infrared spectrum of **1** is shown in Fig. S5†. The broad IR absorption bands at ~3559 and ~3417 cm^{-1} confirm the presence of water molecules. The stretching vibrations ν(Se–O) of the $[SeO_3]^{2-}$ groups appear at 741–688 cm^{-1}, and absorption bands from 437 to 493 cm^{-1} belong to the bending vibrations ν(O–Se–O) of the $[SeO_3]^{2-}$ units. The broad and strong absorption bands in the range of 1442–1295 cm^{-1} and 882–823 cm^{-1} can be assigned to the characteristic absorption of the $[NO]^{3-}$ group.

UV-Vis-NIR Diffuse Reflectance Spectrum

The UV-Vis-NIR absorption spectrum and UV-Vis-NIR diffuse reflectance spectrum reveal that **1** shows little absorption in the wavelength region of 2500–300 nm (Fig. 4 and Fig. S6†). The band gap for **1** is calculated to be 5.53 eV according to Kubelka-Munk function, which is consistent with its transparent color. The cutoff edge in the UV region is therefore 224 nm, which is the shortest value observed among selenite-based NLO materials (Table S4†). The introduction of planar π-conjugated nitrate groups into selenites is conductive to shift the cutoff edges to the UV spectral region and thereby enlarge the band gaps of NLO materials.

LDT Measurements

A wide band gap may be beneficial to obtain a high LDT. Preliminary LDT measurements were performed on the powder samples of **1** together with $AgGaS_2$ as the reference. The results indicate that **1** exhibits large LDT (236.26 MW/cm^2), which is much higher than that of benchmark

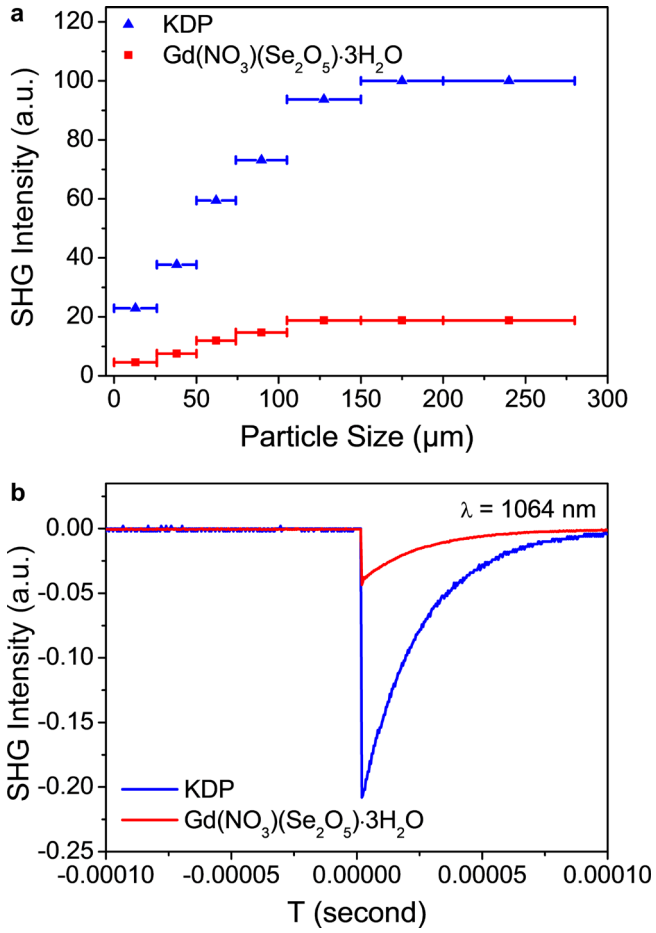

Fig. 5 (a) Phase-matchable curve of $Gd(NO_3)(Se_2O_5)\cdot 3H_2O$ with 1064 nm laser radiation. (b) Oscilloscope traces of the SHG signals for powders of $Gd(NO_3)(Se_2O_5)\cdot 3H_2O$ and KDP in the same particle size range of 105–150 μm.

$AgGaS_2$[52] (2.12 MW/cm^2) (Table S5†). Such an excellent performance indicates that **1** is a promising candidate for high-power NLO application.

SHG Properties

Since **1** crystallizes in the NCS space group $P2_12_12_1$ (No. 19), it is worthwhile to investigate its nonlinear optical properties. The powder NLO properties of **1** were systematically studied as a function of particle size with a Q-switched Nd:YAG laser (1064 nm). As shown in Fig. 5a, the SHG intensity grows gradually as the particle size increases until it reaches a maximum above 150 μm, which indicates that **1** is a phase-matchable crystal. With the same particle size range of 105–150 μm, the SHG efficiency of **1** is 0.20 times that of KDP (Fig. 5b). The relatively weak SHG response can be attributed to the incomplete cancellation of the regional dipole moments associated with $[Se_2O_5]^{2-}$ and $[NO_3]^-$ units (Fig. S7†).

Theoretical Calculations

Theoretical calculations were carried out by density functional theory (DFT) methods to gain further insights into the optical properties of **1**. The band structure of **1** is depicted in Fig. S8†. The valence band maximal (VBM) is placed at G point, while

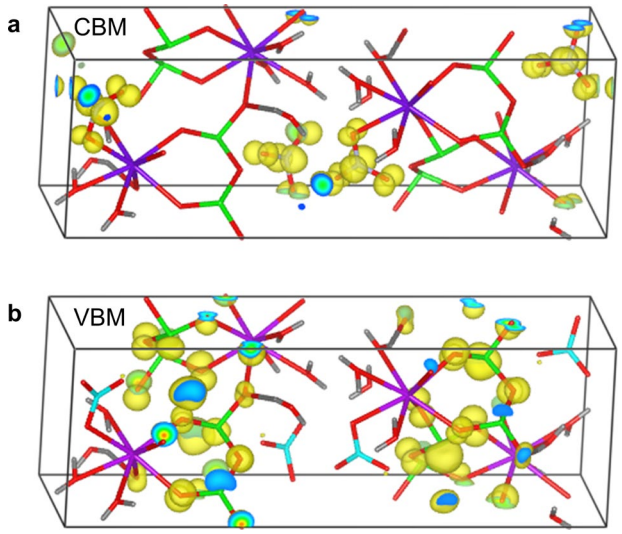

Fig. 6 Wave functions of the conduction band maxima (CBM, (a)) and the valence band maxima (VBM, (b)) for $Gd(NO_3)(Se_2O_5)\cdot 3H_2O$. Color codes: Gd purple, Se green, N blue, O red, H gray.

the conduction band minimal (CBM) is located at X point, which indicates that **1** belongs to an indirect band gap material with the band gap of 3.28 eV. The calculated band gap is much smaller than the experimental value due to the limitation of the DFT methods. To better understand the VBM and CBM, the electron densities of VBM and CBM at G and X points, respectively, for **1** are shown in Fig. 6. The CBM is made up of O 2p and N 2p states localized in the $[NO_3]^-$ unit, while the VBM consists of states from the $[Se_2O_5]^{2-}$ unit. The results demonstrate that the optical diffuse absorption spectrum can be attributed to charge transfer from O 2p state to N 2p and Se 4p states. The density of states (DOS) can be used both to assign the band structure and to understand the interactions among atoms in **1**. The electronic states of Se, N and Gd atoms are fully overlapped with those of O atoms in the energy regions ranging from the VB to CB, showing the strong interactions of Se−O, N−O, and Gd−O bonds in **1** (Fig. S9†). The linear and nonlinear optical properties are mainly determined by the electronic transitions among the states nearby the Fermi level like O 2p, N 2p and a few Se 4p orbitals, indicating that $[SeO_3]^{2-}$ and $[NO_3]^-$ groups are the main contributors to the nonlinear optical response of **1**. The frequency-dependent refractive index curve of **1** is displayed in Fig. 7. The refractive indices follow the order of $n^z > n^y > n^x$, and the birefringence is 0.109 at 1064 nm for the **1**, which is large enough to satisfy the phase matching requirement in the SHG process.

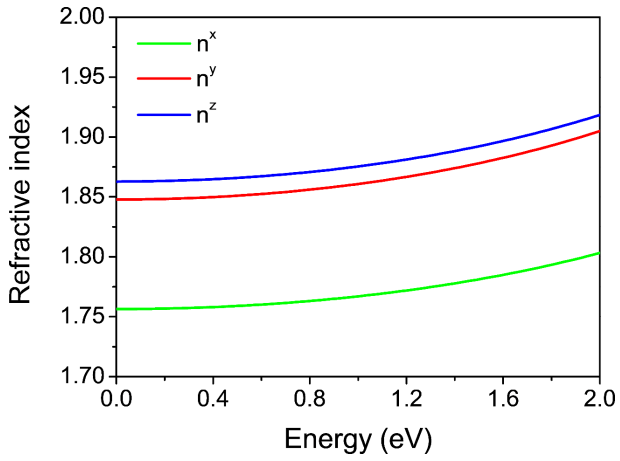

Fig. 7 Calculated refractive indexes of $Gd(NO_3)(Se_2O_5)\cdot 3H_2O$

Conclusions

In summary, the first example of rare-earth metal nitrate-selenite NLO crystal $Gd(NO_3)(Se_2O_5)\cdot 3H_2O$ was successfully synthesized by a facile hydrothermal mean. The crystal structure, NLO performance, and thermal stability of the reported crystalline compound have been investigated. $Gd(NO_3)(Se_2O_5)\cdot 3H_2O$ possesses a pseudo-3D framework consisting of 2D $[Gd(NO_3)(Se_2O_5)]_\infty$ layers. The compound exhibits a SHG response (~0.2 × KDP) at 1064 nm and a large LDT of 236.26 MW/cm^2. Additionally, its unique structure leads to a short UV cutoff edge of 224 nm with an indirect band gap of 5.53 eV, which is the shortest value observed among selenite-based NLO materials. The calculated birefringence is 0.109 at 1064 nm, which is sufficiently large enough to achieve phase matching. This study indicates that the combination of nitrate and selenite as well as rare-earth cation can be a feasible route for the development of NLO materials with short-wavelength cutoff edge, high LDT, moderate SHG response and birefringence.

Acknowledgements

This research was financially supported by the National Natural Science Foundation of China (no. 51432006), the Ministry of Education of China for the Changjiang Innovation Research Team (no. IRT13R24), the Ministry of Education and the State Administration of Foreign Experts Affairs for the 111 Project (no. B13025), the Innovation Program of Shanghai Municipal Education Commission, and the National and Shanghai Postdoctoral Program for Innovative Talents (nos. BX201800216 and 2018192). M. G. H. and C. Z. thank the Australian Research Council for support (DP170100411). The authors thank G. Z. and B. X. L. at FJIRSM for help with the LDT measurements.

Conflicts of interest

The authors declare that they have no conflict of interest.

Notes and references

1 M. Mutailipu, M. Zhang, Z. H. Yang and S. L. Pan, *Acc. Chem. Res.*, 2019, **52**, 791-801.
2 N. Savage, *Nature Photon.*, 2007, **1**, 83-85.
3 T. T. Tran, N. Z. Koocher, J. M. Rondinelli and P. S. Halasyamani, *Angew. Chem. Int. Ed.*, 2017, **56**, 2969-2973.
4 G. H. Zou, C. S. Lin, H. Jo, G. Nam, T. S. You and K. M. Ok, *Angew. Chem. Int. Ed.*, 2016, **55**, 12078-12082.

5 D. H. Lin, M. Luo, C. S. Lin, F. Xu and N. Ye, *J. Am. Chem. Soc.*, 2019, **141**, 3390-3394.
6 J. H. Feng, C. L. Hu, H. P. Xia, F, Kong and J. G. Mao, *Inorg. Chem.*, 2017, **56**, 14697-14705.
7 L. Kang, F. Liang, X. X. Jiang, Z. S. Lin and C. T. Chen, *Acc. Chem. Res.*, 2020, 53, 209-217.
8 H. W. Yu, N. Z. Koocher, J. M. Rondinelli and P. S. Halasyamani, *Angew. Chem. Int. Ed.*, 2018, **57**, 6100-6103.
9 C. Wu, G. Yang, M. G. Humphrey and C. Zhang, *Coord. Chem. Rev.*, 2018, **375**, 459-488.
10 F. Liang, L. Kang, X. Y. Zhang, M. H. Lee, Z. S. Lin and Y. C. Wu, *Cryst. Growth Des.*, 2017, **17**, 4015-4200.
11 J. Lu, Y. K. Lian, L. Xiong, Q. R. Wu, M. Zhao, K. X. Shi, L. Chen and L. M. Wu, *J. Am. Chem. Soc.*, 2019, **141**, 16151-16159.
12 P. F. Gong, S. Z. Zhang, G. M. Song, X. M. Liu and Z. S. Lin, *Chem. Commun.*, 2020, **56**, 643-646.
13 Y. Z. Huang, L. M. Wu, X. T. Wu, L. H. Li, L. Chen and Y. F. Zhang, *J. Am. Chem. Soc.*, 2010, **132**, 12788-12789.
14 C. M. Huang, G. P. Han, H. Li, F. F. Zhang, Z. H. Yang and S. L. Pan, *Dalton Trans.*, 2019, **48**, 6714-6717.
15 Q. Qi, L. Sun, J. Zhang and G. Y. Yang, *Dalton Trans.*, 2017, **46**, 7911-7916.
16 S. G. Zhao, P. F. Gong, L. Bai, X. Xu, S. Q. Zhang, Z. H. Sun, Z. S. Lin, M. C. Hong, C. T. Chen, J. H. Luo, *Nature Commun.*, 2014, **5**, 4019(1)-4019(7).
17 J. H. Huang, C. C. Jin, P. L. Xu, P. F. Gong, Z. S. Lin, J. W. Cheng and G. Y. Yang, *Inorg. Chem.*, 2019, **58**, 1755-1758.
18 C. Wu, L. H. Li, G. Yang, J. L. Song, B. Yan, M. G. Humphrey, L. Zhang, J. D. Shao and C. Zhang, *Dalton Trans.*, 2017, **46**, 12605-12611.
19 S. L. Pan, J. P. Smit, B. Watkins, M. R. Marvel, C. L. Stern and K. R. Poeppelmeier, *J. Am. Chem. Soc.*, 2006, **128**, 11631-11634.
20 C. T. Chen, B. C. Wu, A. D. Jiang, G. M. You, *Sci. Sin., Ser. B*, 1985, **28**, 235-243.
21 C. T. Chen, Y. C. Wu, A. D. Jiang, B. C. Wu, G. M. You, R. K. Li, S. J. Lin, *J. Opt. Soc. Am. B*, 1989, **6**, 616-621.
22 C. T. Chen, Y. B. Wang, B. C. Wu, K. C. Wu, W. L. Zeng and L. H. Yu, *Nature*, 1995, **373**, 322-324.
23 L. Huang, G. H. Zou, H. Q. Cai, S. C. Wang, C. S. Lin and N. Ye, *J. Mater. Chem. C*, 2015, **3**, 5268-5274.
24 X. M. Liu, P. F. Gong, Y. Yang, G. M. Song and Z. S. Lin, *Coord. Chem. Rev.*, 2019, **400**, 213045(1)-213045(13).
25 Y. Song, M. Luo, C. Lin and N. Ye, *Chem. Mater.*, 2017, **29**, 896-903.
26 L. Wang, F. Yang, X. Y. Zhao, L. Huang, D. J. Gao, J. Bi, X. Wang and G. H. Zou, *Dalton Trans.*, 2019, **48**, 15144-15150.
27 E. J. Cho, S. J. Oh, H. Jo, J. Lee, T. S. You, K. M. Ok, *Inorg. Chem.*, 2019, **58**, 2183-2190.
28 L. X. Chang, L. Wang, X. Su, S. L. Pan, R. Hailili, H. W. Yu, Z. H. Yang, *Inorg. Chem.*, 2014, **53**, 3320-3325.
29 H. W. Yu, M. L. Nisbet and K. R. Poeppelmeier, *J. Am. Chem. Soc.*, 2018, **140**, 8868-8876.
30 C. Wu, L. Lin, X. X. Jiang, Z. S. Lin, Z. P. Huang, M. G. Humphrey, P. S. Halasyamani and C. Zhang, *Chem. Mater.*, 2019, **31**, 10100-10108.
31 S. H. Kim, J. Yeon and P. S. Halasyamani, *Chem. Mater.*, 2009, **21**, 5335-5342.
32 H. W. Yu, J. S. Young, H. P. Wu, W. G. Zhang, J. M. Rondinelli and P. S. Halasyamani, *J. Am. Chem. Soc.*, 2016, **138**, 4984-4989.
33 X. L. Cao, C. L. Hu, X. Xu, F. Kong and J. G. Mao, *Chem. Commun.*, 2013, **49**, 9965-9967.
34 F. G. You, F. Liang, Q. Huang, Z. G. Hu, Y. C. Wu and Z. S. Lin, *J. Am. Chem. Soc.*, 2019, **141**, 748-752.
35 S. G. Zhao, Y. Yang, Y. G. Shen, B. Q. Zhao, L. N. Li, C. M. Ji, Z. Y. Wu, D. Q. Yuan, Z. S. Lin, M. C. Hong, J. H. Luo, *Angew. Chem. Int. Ed. Engl.*, 2017, **56**, 540-544.
36 C. Y. Meng, L. Geng, W. T. Chen, M. F. Wei, K. Dai, H. Y. Lu, W. D. Cheng, *J. Alloys Compd.*, 2015, **640**, 39-44.
37 Y. X. Ma, C. L. Hu, B. X. Li, F. Kong, J. G. Mao, *Inorg. Chem.*, 2018, **57**, 11839-11846.
38 Y. G. Chen, N. Yang, X. X. Jiang, Y. Guo and X. M. Zhang, *Inorg. Chem.*, 2017, **56**, 7900-7906.
39 M. Mutailipu, M. Zhang, B. B. Zhang, Z. H. Yang and S. L. Pan, *Chem. Commun.*, **54**, 6308-6311.
40 X. Hao, M. Luo, C. S. Lin, D. H. Lin, L. L. Cao and N. Ye, *Dalton Trans.*, 2019, **48**, 12296-12302.
41 X. L. Chen, F. F. Zhang, Y. J. Shi, Y. Z. Sun, Z. H. Yang and S. L. Pan, *Dalton Trans.*, 2018, **47**, 750-757.
42 G. M. Sheldrick, SHELXS-97: Program for the Solution of Crystal Structures; University of Göttingen: Germany, 1997.
43 N. E. Brese and M. O'Keeffe, *Acta Crystallogr., Sect. B: Struct. Sci.*, 1991, **B47**, 192-197.
44 A. L. Spek, *J. Appl. Crystallogr.*, 2003, **36**, 7-13.
45 W. M. Wendlandt and H. G. Hecht, Reflectance Spectroscopy; Interscience: New York, 1966.
46 S. K. Kurtz and T. T. Perry, *J. Appl. Phys.*, 1968, **39**, 3798-3813.
47 M. J. Zhang, X. M. Jiang, L. J. Zhou and G. C. Guo, *J. Mater. Chem. C*, 2013, **1**, 4754-4760.
48 G. Kresse and J. Furthmuller, *Phys. Rev. B: Condens. Matter. Phy.*, 1996, **54**, 11169-11186.
49 J. P. Perdew, K. Burke and M. Ernzerhof, *Phys. Rev. Lett.*, 1996, **77**, 3865-3868.
50 P. E. Blochl, *Phys. Rev. B: Condens. Matter. Phy.*, 1994, **50**, 17953-17979.
51 G. Kresse and D. Joubert, *Phys. Rev. B: Condens. Matter. Phy.*, 1999, **59**, 1758-1775.
52 B. Tell and H. M. Kasper, *Phys. Rev. B: Solid State*, 1971, **4**, 4455-4459.